PCCP

PAPER

View Article Online
View Journal | View Issue

Cite this: *Phys. Chem. Chem. Phys.*, 2016, **18**, 17997

Effective participation of $Li_4(NH_2)_3BH_4$ in the dehydrogenation pathway of the $Mg(NH_2)_2$–2LiH composite†

G. Amica,*[ab] F. Cova,[ab] P. Arneodo Larochette[ab] and F. C. Gennari[ab]

Received 28th April 2016,
Accepted 7th June 2016

DOI: 10.1039/c6cp02854c

www.rsc.org/pccp

Lithium fast-ion conductors have shown positive effects on the hydrogen storage properties of the Li–Mg–N–H system. In the present work, $Li_4(NH_2)_3BH_4$ doped $Mg(NH_2)_2$–2LiH was formed by milling the $2LiNH_2$–MgH_2–$0.2LiBH_4$ composite and posterior annealing under hydrogen pressure to reduce the kinetic barrier of the Li–Mg–N–H system. The effect of repetitive dehydrogenation/rehydrogenation cycles on the kinetic and thermodynamic performance was evaluated. The dehydrogenation rate in the doped composite was twice that in the un-doped sample at 200 °C, while hydrogenation was 20 times faster. The activation energy decreases by 9% due to the presence of $Li_4(NH_2)_3BH_4$ compared to the un-doped composite, evidencing its catalytic role. The presence of $Li_4(NH_2)_3BH_4$ in the composite stabilized the hydrogen storage capacity after successive sorption cycles. Thermodynamic studies revealed a variation in the pressure composition isotherm curves between the first dehydrogenation cycle and the subsequent. The $Li_4(NH_2)_3BH_4$ doped composite showed a sloped plateau region at higher equilibrium pressure in regard to the flat plateau of the un-doped composite. Detailed structural investigations revealed the effective influence of $Li_4(NH_2)_3BH_4$ in different reactions: the irreversible dehydrogenation in the presence of MgH_2 and the reversible hydrogen release when it reacts with $Li_2Mg_2(NH)_3$. The role of $Li_4(NH_2)_3BH_4$ in improving the dehydrogenation kinetics is associated with the weakening of the N–H bond and the mobile small ion mass transfer enhancement.

1. Introduction

Hydrogen storage remains one of the most challenging technological barriers to the advance of hydrogen economy.[1] Although there are several hydrogen storing methods, the solid-state provides improved volumetric energy densities in comparison with compressed gas or liquid hydrogen, combined with safe and efficient conditions at moderate pressure and temperature. As none of the known hydrides meet simultaneously the required properties for hydrogen storage applications due to several limitations (such as unfavourable thermodynamics, poor kinetics, inability to rehydrogenate or low reversible hydrogen storage capacity), intensive investigations have been carried out to search for new materials.[2–20] Recently, complex metal hydride storage systems, such as borohydrides,[3–5] alanates[6–8] and amide-hydrides,[9–20] began to be considered as promising materials for safe and efficient hydrogen storage. Among the studied systems, the $Mg(NH_2)_2$–LiH composite has been proved to be a propitious candidate for onboard applications due to its good reversibility, moderate operating temperatures, relatively high hydrogen storage capacity (5.5 wt% H) and suitable ΔH (~44.1 kJ mol^{-1} H_2), determining a desorption temperature lower than 100 °C at atmospheric pressure.[11,13,17–20] Hu *et al.*[18] revealed that the hydrogenation/dehydrogenation pathway of this composite was a two-step reaction which involves the formation and consumption of a ternary imide $Li_2Mg_2(NH)_3$, according to the following pathway:

$$2Mg(NH_2)_2 + 3LiH \rightarrow Li_2Mg_2(NH)_3 + LiNH_2 + 3H_2 \quad (1)$$

$$Li_2Mg_2(NH)_3 + LiNH_2 + LiH \rightarrow 2Li_2Mg(NH)_2 + H_2 \quad (2)$$

In all:

$$2Mg(NH_2)_2 + 4LiH \rightarrow 2\ Li_2Mg(NH)_2 + 4H_2\ 5.5\ wt\% \quad (3)$$

However, due to kinetic constraints, temperatures over 200 °C are required to achieve reasonable desorption rates. Kinetic studies revealed that the rate-limiting step for the dehydrogenation

[a] *Consejo Nacional de Investigaciones Científicas y Técnicas (CONICET) and Centro Atómico Bariloche (CNEA), Av. Bustillo 9500, R8402AGP, S. C. de Bariloche, Río Negro, Argentina. E-mail: guillerminaamica@gmail.com; Fax: +54 294 4445190; Tel: +54 294 4445712*

[b] *Instituto Balseiro, Universidad Nacional de Cuyo, Argentina*

† Electronic supplementary information (ESI) available. See DOI: 10.1039/c6cp02854c

process of $Li_2Mg(NH)_2$ is controlled by diffusion.[20,21] Adding catalysts, such as alkali metal compounds[22–25] and metal borohydrides,[26,27] improves the thermodynamic properties of the system and lowers operating temperatures. Yang *et al.*[28] reported that due to the formation of $Li_4(NH_2)_3BH_4$ (low melting temperature ionic liquid), the composite $2LiNH_2$–MgH_2–$LiBH_4$ exhibited a ''self-catalyzing'' reaction pathway that resulted in faster kinetics, lower desorption temperatures and ammonia release suppression. Later, Hu *et al.* proved that by adding 10% $LiBH_4$ the heat of dehydrogenation was reduced from 40 to 36.5 kJ mol^{-1}.[27] Moreover, it was reported that other borohydrides, such as $Ca(BH_4)_2$ and $Mg(BH_4)_2$, have similar effects as catalysts in this composite since they turn to $LiBH_4$, with the posterior formation of $Li_4(NH_2)_3BH_4$ during hydrogen sorption.[29–31] Cao *et al.* have studied the additive effects of $LiBH_4$, LiI and LiBr on the $2Mg(NH_2)_2$–3LiH composite. The reaction enthalpy was successfully tailored by stabilizing the dehydrogenated product $LiNH_2$ in Ec (1) due to the formation of more stable compounds $Li_4(NH_2)_3BH_4$, $Li_3(NH_2)_2I$, and $Li_2(NH_2)Br$.[32] In fact, besides the $Li_4(NH_2)_3BH_4$ formation, $LiNH_2$ can also be combined with lithium halides to form lithium fast-ion conductors, such as $Li_4(NH_2)_3Cl$, $Li_7(NH_2)_6Br$ and $Li_3(NH_2)_2I$, as it was revealed by Anderson *et al.*[33] These amide-halide phases display promising hydrogen storage properties because, in the presence of LiH, they reversibly release hydrogen and NH_3 emission is practically negligible. Li *et al.* showed that the *in situ* formation of $Li_7(NH_2)_6Br$ improves the hydrogen storage performance of the $LiNH_2$–MgH_2 system by reducing the dehydrogenation temperature, increasing the dehydrogenation rate and suppressing ammonia emission.[34] By adding LiCl to $LiNH_2$ or $Mg(NH_2)_2$, the effect of the $Li_4(NH_2)_3Cl$ formation on the hydrogen storage performance becomes complex. For example, a negative effect of LiCl addition to the $Mg(NH_2)_2$–2LiH composite has been recently presented.[35] The *in situ* formation of $Li_4(NH_2)_3Cl$ during hydrogen cycling at 200 °C deteriorated the hydrogen storage capacity and the dehydrogenation rate due to the consumption of $LiNH_2$ by a competitive reaction. In addition, it was further shown that the thermodynamic stability of the $Li_4(NH_2)_3Cl$–3LiH composite was higher than that of the $Mg(NH_2)_2$–2LiH one and similar to the $LiNH_2$–LiH system.[36] In contrast, adding $AlCl_3$ (0.03 mol) to $LiNH_2$–LiH enhances its hydrogen storage properties due to the incorporation of Al^{3+} and Cl^- to the Li_2NH-type structure.[37] In fact, about 4.5–5.0 wt% of hydrogen was reversibly stored under cycling at 275 °C, throughout a process which avoided ammonia release. In a further study, cubic and hexagonal amide-chloride phases in the Li–Al–N–H–Cl system were observed using high $AlCl_3$ concentration (0.08 and 0.13 mol) along with mild thermal treatments in controlled environments.[38] These amide-chloride phases improved dehydrogenation properties compared to $LiNH_2$–LiH, providing an alternative reaction pathway.[39] Due to the different properties among $Li_4(NH_2)_3BH_4$, $Li_4(NH_2)_3Cl$ and $Li_2(NH_2)Br$ phases, their hydrogen sorption properties in Li–N–H and Li–Mg–N–H systems could vary.

To evaluate the effect of $Li_4(NH_2)_3BH_4$ on the hydrogen storage performance of $Mg(NH_2)_2$–2LiH, the $0.7Mg(NH_2)_2$–$1.4LiH$–$0.2Li_4(NH_2)_3BH_4$ composite was prepared by milling $2LiNH_2$–MgH_2–$0.2LiBH_4$ and posteriorly heating it at 200 °C under 6.0 MPa of hydrogen. The hydrogen sorption and thermodynamic properties of this composite were studied and then compared to those of pristine $Mg(NH_2)_2$–2LiH. The result of repetitive dehydrogenation/rehydrogenation cycles on the kinetic and thermodynamic behaviour at 200 °C was evaluated. The role of $Li_4(NH_2)_3BH_4$ in the reaction pathway and the hydrogen storage properties of the Li–Mg–N–H were clarified.

2. Experimental

2.1 Synthesis of the composites

The starting materials were commercial $LiNH_2$ (Aldrich, 95%), MgH_2 (Aldrich, 98%), and $LiBH_4$ (Aldrich, 90%). Due to the high reactivity of the samples, they were handled in a MBraun Unilab argon-filled glove box, with oxygen and moisture levels lower than 1 ppm. For all studies, high purity hydrogen (Linde, 99.999%) and argon (Linde, 99.999%) were used. The sample was prepared by mechanical milling of $2LiNH_2$–MgH_2 (LM) and $2LiNH_2$–MgH_2–$0.2LiBH_4$ (LMB), using a sequence of 15 min milling and 10 min pause in a planetary ball mill (Fritsch Pulverisette 6). The milling conditions were 500 rpm with a ball to powder mass ratio of 53 : 1 for 20 h. To improve the powder mixing and eliminate possible dead zones, the material was manually mixed after 1 h, 3 h, 5 h, 10 h and 15 h.

2.2 Characterization of the composites

The structural, thermal and hydrogen storage properties of the as-milled and as-cycled samples were studied using differential scanning calorimetry (DSC, TA 2910 calorimeter), X-ray powder diffraction (XRPD, PANalytical Empyrean), Fourier transform infrared spectroscopy (FTIR, Perkin Elmer Spectrum 400 with MCT detector), thermogravimetry (TG-HP50, TA Instruments) and a Sieverts-type apparatus.

Structural information of the samples was obtained by XRPD (Cu Kα radiation, graphite monochromator) and FTIR analyses. During the XRPD data collection, all the samples were kept under an Ar atmosphere using an airtight holder to prevent any reaction between samples and air. For IR spectroscopy measurements, the samples were ground with dry KBr under a purified argon atmosphere, pressed to pellets and placed in a specially designed airtight cell. Handling was done inside the glove box to avoid contact with air. Solid state IR spectra were obtained in the range of 4000–800 cm^{-1} with a resolution of 4 cm^{-1}. The gases released after milling and during dehydrogenation of the samples were collected in a degassed quartz optical cell with KBr windows. The gas phase spectra at room temperature were taken, with a resolution of 0.5 cm^{-1}. A minor amount of NH_3 emission was detected by gas-FTIR analysis during sample LM dehydrogenation at 200 and 250 °C.

The thermal behaviour of the samples was studied by DSC using heating ramps between 1 and 10 °C min^{-1} and an argon flow rate of 122 ml min^{-1}. About 3–5 mg of sample was loaded

into aluminium capsules closed in a glove box. Kissinger's method was employed to determine the activation energy (E_a):

$$\ln(\beta\ T_m^{-2}) = \ln(A\ R\ E_a^{-1})\ (-E_a\ R^{-1}\ T_m^{-1}) \quad (4)$$

where T_m is the peak temperature at which the maximum reaction rate is attained, β is the heating rate, A is a constant and R is the gas constant. Pressure-composition isotherms (PCIs) and hydrogen sorption kinetics were obtained using modified Sieverts-type equipment, coupled with a mass flow controller. The sample was transferred into the glove box inside a stainless reactor which was connected to the Sieverts device. Before the first dehydrogenation, for both thermodynamic and kinetic measurements, the sample was heated up to the reaction temperature (200 °C) under hydrogen pressure (6.0 MPa) and kept at this temperature for 30 min. Dehydrogenation curves were obtained at 200 °C with a hydrogen back pressure of 0.05 MPa. The rehydrogenation curves were measured at 200 °C at a constant hydrogen pressure of 6.0 MPa. The amount of absorbed/desorbed hydrogen was determined with a relative error ±5%. As regards PCI,[35] a stationary state at 200 °C in each sample was required before measuring PCI at other temperatures. The hydrogen contents reported in this paper are expressed as wt% considering the total mass of each mixture. Sample composition after annealing and PCI measurements was studied by PXRD and the Rietveld method.[40] A pseudo-Voigt shape was assumed for the refinement. The background introduced by the sample holder was initially set by hand and refined in each run. Fullprof software[41] was employed to obtain the ATZ coefficient for each PXRD measurement, which enabled us to perform the quantitative phase analysis for each partially absorbed sample.

3. Results and discussion

3.1 Synthesis of $Li_4(NH_2)_3BH_4$ modified $Mg(NH_2)_2$–LiH by ball milling and thermal treatment

$Mg(NH_2)_2$ is intended to be obtained by ball milling the $LiNH_2$–MgH_2 initial mixture under the experimental conditions described above. The following equation indicates the expected reaction to allow the formation of the $Mg(NH_2)_2$–2LiH composite (LM):

$$2LiNH_2(s) + MgH_2(s) \rightarrow Mg(NH_2)_2(s) + 2LiH(s) \quad (5)$$

$Mg(NH_2)_2$ formation is identified by its characteristic N–H vibrations at 3325 cm^{-1} and 3271 cm^{-1} (Fig. 1A), as well as residual $LiNH_2$ by its characteristic bands at 3313 cm^{-1} and 3258 cm^{-1}. The detection of a broad band at 3180 cm^{-1} can be associated with $Li_2Mg(NH)_2$ (Fig. 1A). Although after milling the XRPD pattern of the pristine sample reveals a low crystallinity which does not allow us to clearly identify any amides (Fig. 1B), crystalline MgH_2 and LiH are easily distinguished.

After submitting the sample LM to thermal treatment under a hydrogen pressure of 0.6 MPa for 0.5 h at 200 °C, the crystallinity of the sample improves. The FTIR bands of the phases $Mg(NH_2)_2$ and $LiNH_2$ can be identified (Fig. 1A). The characteristic band of $Li_2Mg(NH)_2$ disappears, suggesting complete

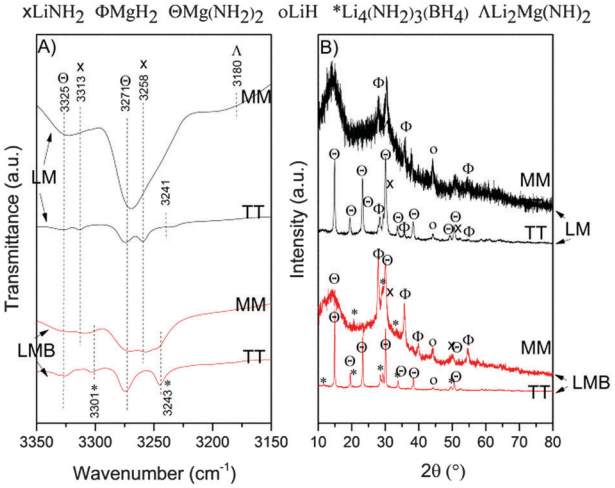

Fig. 1 FTIR spectra (A) and XRPD patterns (B) of the LM and LMB samples after mechanical milling (MM) and thermal treatment (TT).

hydrogenation, and the band of its decomposition products at 3241 cm^{-1} arises.[42] Additionally, MgH_2 and LiH can be detected by XRPD (Fig. 1B).

To modify the kinetic and/or thermodynamic behaviour of the pristine material, 0.2 $LiBH_4$ was added to the $LiNH_2$–MgH_2 (LMB) composite. Structural information of the LMB sample was obtained by FTIR and XRPD analyses. The identification of a broad band at 2300 cm^{-1} by FTIR indicates the presence of B–H type bonds (see Fig. S1, ESI†). The formation of $Mg(NH_2)_2$ and the presence of residual $LiNH_2$ are demonstrated by FTIR (Fig. 1A). As for the LM sample, an excess of MgH_2 is detected by XRPD. Furthermore, the identification of the most intense diffraction peaks from the phase $Li_4(NH_2)_3BH_4$ proves its formation during milling (Fig. 1B), according to the following equation:[46]

$$1/3\ LiBH_4(s) + LiNH_2(s) \rightarrow 1/3\ Li_4(NH_2)_3BH_4(s) \quad (6)$$

The LM sample was submitted to the same thermal treatment and both, $Mg(NH_2)_2$ and $Li_4(NH_2)_3BH_4$ (3301 and 3243 cm^{-1}), were detected by FTIR. Neither $LiNH_2$, MgH_2 nor $LiBH_4$ were identified as unreacted phases. So, $Mg(NH_2)_2$–LiH was synthesised in LM and LMB samples by mechanical milling of $LiNH_2$ and MgH_2 followed by thermal treatment for 30 min at 200 °C under 6.0 MPa of hydrogen. The main difference between both composites is the formation of the new phase $Li_4(NH_2)_3BH_4$ in LMB during mechanical milling. Moreover, it is important to highlight that no excess of any reactive was detected in the LMB sample. These results are in agreement with previous studies, which have demonstrated that the addition of $LiBH_4$ contributes to the formation/recrystallization of $Mg(NH_2)_2$.[43]

In order to quantify the amount of each phase and determine the synthesis efficiency, Rietveld refinements were carried out for LM and LMB samples after thermal treatment. In the former, the relation between the molar amount of $Mg(NH_2)_2$ and $LiNH_2$ was increased according to the thermal treatment

duration, suggesting a reaction displacement. For 0.5 h of annealing, the phase molar ratio ($Mg(NH_2)_2/LiNH_2$) was 59/41, whereas for 23 and 126 h it became 68/32 and 86/14, respectively. As regards the LMB sample, none of the initial components were detected after 0.5 h of annealing. Then, it can be assumed that the amount of $Mg(NH_2)_2$ will not vary with the treatment duration. In this case, the molar ratio $g(NH_2)_2/Li_4(NH_2)_3BH_4$ was 79/21.

It is worth mentioning that (for calculations) only amides and related compounds ($Li_4(NH_2)_3BH_4$ in particular) were considered, excluding LiH. Therefore, clearer results and a direct comparison between the compounds of interest can be achieved.

3.2 Hydrogen storage reversibility of the $Mg(NH_2)_2$–LiH–$Li_4(NH_2)_3BH_4$ composite: kinetics and cycling behaviour

To evaluate the influence of $Li_4(NH_2)_3BH_4$ on the hydrogen sorption behaviour, volumetric measurements were carried out. As a representative performance, Fig. 2A and B show the dehydrogenation/rehydrogenation curves of the second cycle for samples LM and LMB. Similar behaviour was observed after several cycles (Fig. S2, ESI†). Hydrogen release rates evidence the beneficial effect of $Li_4(NH_2)_3BH_4$ on the composite. Considering the slope between 0.02 wt% and 0.2 wt% as a function of time for the 2nd cycle, a dehydrogenation rate of 0.54 ± 0.05 wt% min^{-1} was obtained for LM, in comparison with 1.03 ± 0.05 wt% min^{-1} for LMB, which shows that the dehydrogenation rate in LMB is twice that in LM (Fig. 2A). Regarding absorptions, the rate increase is even higher. Sample LM needs more than 30 minutes to achieve 90% of its total capacity, whereas sample LMB requires only 75 seconds (Fig. 2B). On the other hand, the previous formation of $Li_4(NH_2)_3BH_4$ during synthesis induces an experimental loss of approximately 10% of its capacity. This value is lower than the theoretical one (34%), calculated considering the $Mg(NH_2)_2$ formation (eqn (5)) with the amount of $LiNH_2$ that remains after reacting with the $LiBH_4$ additive (eqn (6)). Then, the collected evidence suggests that there might be another reaction as a source of hydrogen. For comparative purposes, the kinetic behaviour of both samples was studied after several consecutive cycles of hydrogen sorption. As an overall characteristic, both the hydrogen storage capacity and the dehydrogenation rate were reduced.

In terms of stability, it can be noticed that the hydrogen desorption capacity of the system LM decreases after the tenth cycle. Remarkably, this negative effect is reduced due to the formation of $Li_4(NH_2)_3BH_4$ in the $Mg(NH_2)_2$–LiH composite. As shown in Fig. 3A, sample LMB was exposed to 30 consecutive cycles of dehydrogenation and rehydrogenation confirming stability improvement in the hydrogen storage capacity with cycling. Besides, the dehydrogenation rate decreases with cycling (Fig. 3B). The dehydrogenation rate in cycle 30 was 56% lower compared to that in cycle 2.

Considering that the formation of $Li_4(NH_2)_3BH_4$ in the pristine Li–Mg–N–H system improves the sorption rates, dehydrogenation activation energy of sample LMB was calculated by Kissinger's method and compared with sample LM (Fig. 4). DSC curves (Fig. 4A and B) agree with previously reported shapes: an endothermic peak associated with the $Mg(NH_2)_2$ decomposition for both samples and an exothermic peak due to the recrystallization of $Mg(NH_2)_2$ in the case of sample LMB. A previous work showed that the recrystallization of $Mg(NH_2)_2$ was facilitated due to the addition of $LiBH_4$.[43] In our case, this process is favoured by the formation of $Li_4(NH_2)_3BH_4$ in the as-milled LMB sample. Using several DSC curves at different heating rates (1, 2, 3, 5 and 10 °C min^{-1}), the maximum reaction rate temperatures were determined. Kissinger's plots, *i.e.* the dependency of $\ln(\beta\, T_m^{-2})$ upon (T_m^{-1}), are displayed in Fig. 4C. The apparent activation energies obtained by linear fitting for LM and LMB samples are 160 ± 10 kJ mol^{-1} and 146 ± 6 kJ mol^{-1}, respectively. There is a reduction (9%) in the activation energy value due to the presence of $Li_4(NH_2)_3BH_4$ in the Li–Mg–N–H system, which suggests a catalytic effect. The reported values of E_a for the $Mg(NH_2)_2$–2LiH composite are diverse, ranging from 102 kJ mol^{-1}[44] to 149.9 kJ mol^{-1}.[43] The wide range of values E_a found in the literature could be related to the variety of factors that influence heterogeneous solid-state reactions, as for example the size of $Mg(NH_2)_2$ particles,[14]

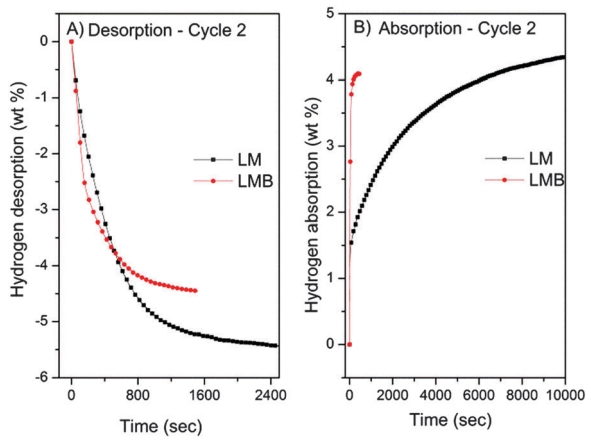

Fig. 2 Second cycle of dehydrogenation (A) and rehydrogenation (B) at 200 °C of the LM and LMB samples. Absorption hydrogen pressure: 6.0 MPa; desorption hydrogen pressure: 0.05 MPa.

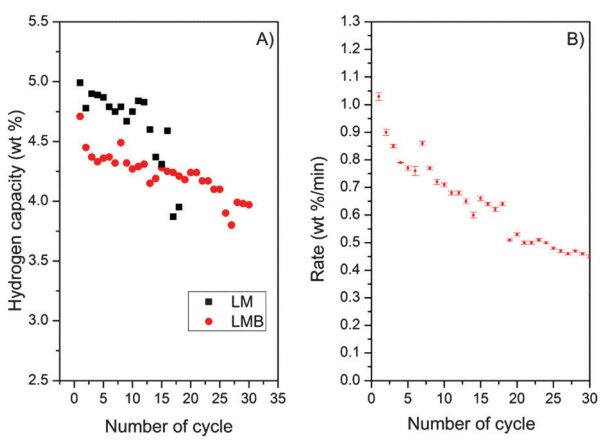

Fig. 3 Hydrogen storage capacity of samples LM and LMB during cycling under hydrogen (A) and dehydrogenation rate of sample LMB *vs.* number of cycles (B).

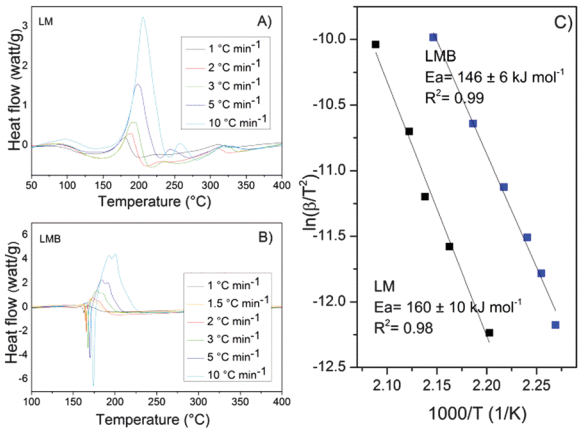

Fig. 4 Kissinger's plots of samples LM and LMB after milling (C); DSC curves collected at different heating rates (1, 2, 3, 5 and 10 °C min^{-1}) for samples LM (A) and LMB (B).

which hinder the direct comparison among them. However, it is possible to compare the effect of an additive introduced to the Li–Mg–N–H system using the same synthesis procedure and studied under the same experimental conditions.

3.3 Hydrogen sorption pathways of the $Mg(NH_2)_2$–LiH–$Li_4(NH_2)_3BH_4$ composite

In order to elucidate the chemical interactions occurring in the dehydrogenation/rehydrogenation processes and to study the structural changes of the LM and LMB samples, a combination of FTIR and XRPD techniques was used. Fig. 5 shows the FTIR spectra and XRPD patterns of the absorbed and desorbed samples after several cycles based on *ex situ* measurements. To simplify the analysis, all phases detected by XRPD and FTIR after milling, thermal treatment and hydrogen cycling have been summarized in Table 1 from the FTIR spectrum of the absorbed state of sample LM shown in Fig. 1 and 5, $Mg(NH_2)_2$ and $LiNH_2$ are clearly identified (Fig. 5A). Furthermore, the

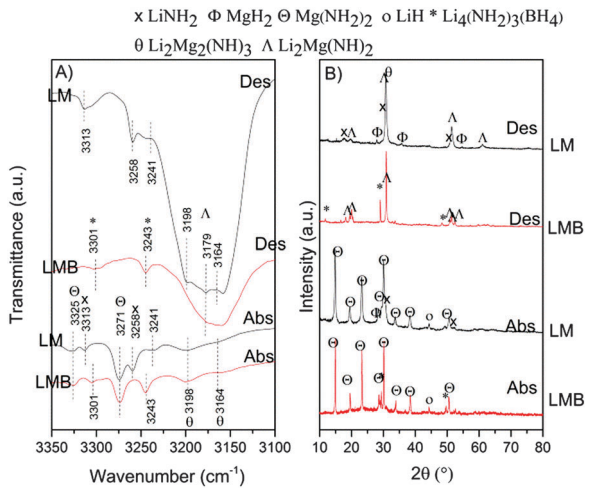

Fig. 5 FTIR spectra (A) and XRPD patterns (B) of the absorbed and desorbed states of the LM and LMB samples.

bands at 3198 cm^{-1} and 3164 cm^{-1} can be attributed to the presence of $Li_2Mg_2(NH)_3$, evidencing the incomplete rehydrogenation of the system. In addition, MgH_2 and LiH were identified by XRPD (Fig. 5B). The band at 3239 cm^{-1} refers to decomposition products of $Li_2Mg(NH)_2$.[42] For sample LMB, $Mg(NH_2)_2$, $Li_4(NH_2)_3BH_4$ and $Li_2Mg_2(NH)_3$ were identified by FTIR and XRPD measurements and the most intense peaks of LiH were also detected. Both samples were afterwards partially rehydrogenated but only the initial $LiNH_2$ and MgH_2 phases remained in sample LM. This is in agreement with previous results (Fig. 1), which indicate that $LiBH_4$ addition favours the formation of $Mg(NH_2)_2$ and the consumption of $LiNH_2$ by reaction (2).

In the desorbed state of the LM sample, $Li_2Mg_2(NH)_3$, $Li_2Mg(NH)_2$ and $LiNH_2$ were detected. Contrastingly, for the dehydrogenated LMB sample, only $Li_4(NH_2)_3BH_4$ and $Li_2Mg(NH)_2$ were identified, which evidences $Mg(NH_2)_2$ complete dehydrogenation. On the basis of these results and in agreement with previous studies on $Mg(NH_2)_2$ decomposition,[17] the following reactions are expected to proceed during dehydrogenation of the LM and LMB samples:

$$2Mg(NH_2)_2(s) + 3LiH(s) \rightarrow LiNH_2(s) + Li_2Mg_2(NH)_3(s) + 3H_2(g) \quad (7)$$

$$Li_2Mg_2(NH)_3(s) + LiNH_2(s) + LiH(s) \rightarrow 2Li_2Mg(NH)_2(s) + H_2(g) \quad (8)$$

The theoretical amount of hydrogen released in reactions (7) and (8) is about 4.1 and 1.4 wt%, respectively. If reaction (8) is not complete, the resultant dehydrogenated solid should contain a mixture of $Li_2Mg_2(NH)_3$, $Li_2Mg(NH)_2$ and $LiNH_2$. This is the case of the LM sample, in which the initial hydrogen storage capacity is about 5.0 wt% and it decreases with hydrogen cycling (see Fig. 3).

To define the role of $Li_4(NH_2)_3BH_4$ in the LMB sample, the reactions which occur from ball milling of $2LiNH_2$–MgH_2–$0.2LiBH_4$ to dehydrogenation must be evaluated considering the mole ratio of each phase. As it has been previously explained (Fig. 1), the additive $LiBH_4$ (0.2 mol) completely reacts with $LiNH_2$ (0.6 mol) during milling and thermal treatment through reaction (6), forming $Li_4(NH_2)_3BH_4$ (0.2 mol). The remnant $LiNH_2$ (1.4 mol) is available to form $Mg(NH_2)_2$ (0.7 mol) according to reaction (5). An excess of MgH_2 (0.3 mol) should have been observed but it was undetectable by XRPD (Fig. 1). Considering reactions (7) and (8) exclusively during dehydrogenation, a hydrogen capacity of 2.7 and 0.9 wt% should be, respectively, obtained (3.6 wt% in total). This value is lower than the hydrogen storage capacity obtained by kinetic measurements (higher than 4.0 wt%, Fig. 3) and it suggests that there must be another reaction involved in hydrogen release. Moreover, the presence of $Li_4(NH_2)_3BH_4$ in the dehydrogenated and hydrogenated state (Table 1) indicates that it only acts as a catalyst. However, its role in the hydrogen sorption process is complex and additional considerations are required. In the following section, possible reactions involving $Li_4(NH_2)_3BH_4$ will be analysed.

Table 1 Species after mechanical milling, thermal treatment and hydrogen sorption of the LM and LMB samples

	Mechanical milling		Thermal treatment		Hydrogenation		Dehydrogenation	
Sample	FTIR	XRPD	FTIR	XRPD	FTIR	XRPD	FTIR	XRPD
LM	$Mg(NH_2)_2$ $LiNH_2$ $Li_2Mg(NH)_2$	$Mg(NH_2)_2$ MgH_2 LiH	$Mg(NH_2)_2$ $LiNH_2$	$Mg(NH_2)_2$ $LiNH_2$ MgH_2 LiH	$Mg(NH_2)_2$ $LiNH_2$ $Li_2Mg_2(NH)_3$	$Mg(NH_2)_2$ $LiNH_2$ MgH_2 $Li_2Mg_2(NH)_3$ LiH	$LiNH_2$ $Li_2Mg_2(NH)_3$ $Li_2Mg(NH)_2$	$LiNH_2$ $Li_2Mg_2(NH)_3$ $Li_2Mg(NH)_2$ MgH_2
LMB	$Mg(NH_2)_2$ $LiNH_2$ $Li_4(NH_2)_3BH_4$	$Mg(NH_2)_2$ MgH_2 LiH	$Mg(NH_2)_2$ $Li_4(NH_2)_3BH_4$	$Mg(NH_2)_2$ $Li_4(NH_2)_3BH_4$ LiH	$Mg(NH_2)_2$ $Li_4(NH_2)_3BH_4$ $Li_2Mg_2(NH)_3$	$Mg(NH_2)_2$ LiH $Li_4(NH_2)_3BH_4$ $Li_2Mg_2(NH)_3$	$Li_4(NH_2)_3BH_4$ $Li_2Mg(NH)_2$	$Li_4(NH_2)_3BH_4$ $Li_2Mg(NH)_2$

3.4 Thermodynamic studies of the $Mg(NH_2)_2$–LiH–$Li_4(NH_2)_3BH_4$ composite

In order to evaluate the thermodynamic stability of the LMB composite and to compare it with LM, pressure–composition-isotherms (PCIs) of dehydrogenation and rehydrogenation were obtained (Fig. 6). It is worth highlighting that for both samples the first dehydrogenation was different from the subsequent. There is an apparent change in the starting material during the first cycle and it reaches a stationary state as from the second/third cycle (Fig. 6A and B). For sample LM, all PCI curves showed a flat plateau. There is a clear increment of the equilibrium pressure between the first (~1.5 MPa) and the second cycle (~1.8 MPa) whereas a nearly constant value is noticed from the third PCI curve onwards (Fig. 6A). According to the information in Table 1, there is a difference between the phases observed after thermal treatment (starting point for the first PCI) and the absorbed state (starting point of the second PCI). Besides, the presence of $Mg(NH_2)_2$, $LiNH_2$ and MgH_2, $Li_2Mg_2(NH)_3$ can be related to incomplete rehydrogenation of the system. As for the consecutive cycles, this intermediate imide can be always observed before dehydrogenation and it may be responsible for the equilibrium pressure increase. After being stabilized by cycling at 200 °C, the LM sample PCI displays a clear plateau of ~2.2 wt% at about 1.8 MPa of hydrogen pressure.

As regards sample LMB, the presence of $Li_4(NH_2)_3BH_4$ influences the equilibrium hydrogen pressure and the PCI shape. The first isotherm displays a flat plateau at ~2.3 MPa of hydrogen pressure, which is higher than that for the LM sample (~1.5 MPa). In addition, there is a visible change in the shape of the PCI with cycling (Fig. 6B) since from the second cycle onwards, the PCI exhibits a sloped plateau, which indicates that the material constitution changes during dehydrogenation.

Once the stationary state is reached at 200 °C, the PCI corresponding to LMB shows a sloped plateau shifting from ~1.8 MPa to ~3.0 MPa, with 2.6 wt% of hydrogen in the plateau region. Thus, the presence of $Li_4(NH_2)_3BH_4$ increases the equilibrium pressure with respect to the LM sample, both in the first cycle as well as in the posterior ones. On the other hand, in the first cycle the starting material consists of $Mg(NH_2)_2$ and $Li_4(NH_2)_3BH_4$ (flat plateau) whereas after cycling $Li_2Mg_2(NH)_3$ is formed due to the incomplete rehydrogenation (sloped plateau). Hence, the $Li_4(NH_2)_3BH_4$ observed before desorption could indicate that there is a correlation between this phase and the sloped plateau. A possible explanation could be related to the interaction of this compound with $Li_2Mg_2(NH)_3$, according to the following reaction:

$$1/3Li_4(NH_2)_3BH_4(s) + Li_2Mg_2(NH)_3(s) + LiH \rightarrow 2Li_2Mg(NH)_2(s) + 1/3\ LiBH_4(s) + H_2(g) \quad (9)$$

In addition to the dehydrogenation of $Mg(NH_2)_2$ *via* reaction (7), reaction (9) could occur from the beginning of the second cycle (PCI or kinetic curve), due to the simultaneous presence of $Li_2Mg_2(NH)_3$ and $Li_4(NH_2)_3BH_4$. The complete consumption of $Li_2Mg_2(NH)_3$ in the dehydrogenated state is in agreement with reaction (9) which, according to the maximum amount of $Li_4(NH_2)_3BH_4$ available, provides extra H_2 (1.6 wt%). Moreover, the $LiBH_4$ obtained by reaction (9) is available to react with $LiNH_2$ produced by reaction (7) and to form $Li_4(NH_2)_3BH_4$ again. The *in situ* formation of $Li_4(NH_2)_3BH_4$ is a fast process, as reported by Hu *et al.*[42] Afterwards, reactions (7) and (9) take place mediated by reaction (6). The removal of $LiNH_2$ (reaction (7)) and $LiBH_4$ (reaction (9)) favours both forward reactions, according to Le Chatelier's principle.

To explain the amount of hydrogen released in the first cycle, additional experiments were performed. The PCI curve at

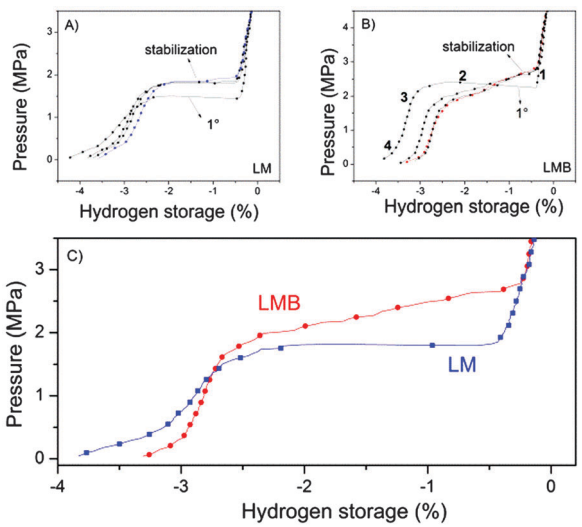

Fig. 6 Cycling of PCIs at 200 °C of the LM (A) and LMB (B) samples; stationary state of PCIs at 200 °C of samples LM and LMB (C).

200 °C was measured using different samples and each one was stopped at variable hydrogen contents (points 1, 2, 3 and 4 in Fig. 6B) to determine both the nature and the proportion of the crystalline phases by the Rietveld method (Table S1 and Fig. S3, ESI†).

After thermal treatment, *i.e.* the initial state of the first PCI, sample LMB contained 32% $Mg(NH_2)_2$, 64% LiH and 6% $Li_4(NH_2)_3BH_4$ (mol%). These values are in agreement, within the experimental error, with the theoretical values expected according to reactions (5) and (6). In the middle of the plateau, $Mg(NH_2)_2$ partially decomposes into $Li_2Mg_2(NH)_3$. It is worth pointing out that the relative proportion of $Li_4(NH_2)_3BH_4$ is almost constant as desorption progresses (see Table S1, ESI†). In addition, although no crystalline $LiNH_2$ could be observed by XRPD, it was detected by FTIR (Fig. S4, ESI†). At the end of the plateau zone, $Li_2Mg_2(NH)_3$ and $Li_2Mg(NH)_2$ were identified. After complete dehydrogenation, a mixture of α and β-$Li_2Mg(NH)_2$ phases and $Li_4(NH_2)_3BH_4$ are still present. According to Rietveld analysis, the amount of $Li_4(NH_2)_3BH_4$ at the end and the beginning of the PCI is similar. This compound could react with the excess of MgH_2 according to:

$$Li_4(NH_2)_3BH_4 + 3MgH_2(s) \rightarrow 3Li_2Mg(NH)_2(s) + 2LiBH_4(s) + 6H_2(s) \quad (10)$$

$$Li_4(NH_2)_3BH_4(s) + 3MgH_2(s) \rightarrow 3Mg(NH_2)_2(s) + 2LiBH_4(s) + 6LiH(s) \quad (11)$$

Considering the maximum theoretical amount of $Li_4(NH_2)_3BH_4$, 1.6 wt% can be released through reaction (10). On the other hand, reaction (11) generates an extra amount of $Mg(NH_2)_2$, which decomposes according to reactions (7) and (8). Reactions (10) and (11) were previously observed during heating of the as-milled $2LiNH_2$–MgH_2–$LiBH_4$ mixture under argon flow.[28] In particular, as temperature increased, $Li_4(NH_2)_3BH_4$ melted favouring the reaction with MgH_2 and releasing hydrogen (reaction (10)). In this study, reaction (10) only occurs during the first desorption cycle due to the availability of un-reacted MgH_2 and provides an extra amount of hydrogen release.

The equilibrium pressures during hydrogen desorption at different temperatures (180–240 °C) were measured for both samples (Fig. 7A and B). The non-lineal behavior insinuates that low temperatures hinder equilibrium conditions and that faster kinetics allows better measurements. The dehydrogenation enthalpy was estimated for samples LM and LMB by lineal fitting of the high temperature data. Considering the three highest temperatures, the dehydrogenation enthalpies obtained were 51 ± 4 kJ mol^{-1} and 42 ± 2 kJ mol^{-1}, respectively, the latter being close to the theoretical value. This insinuates that variations in ΔH may be ascribed to measuring methods and the difficulty in achieving thermodynamic conditions. By comparison, a clear thermodynamic destabilization of the system is not observed. On the other hand, thermodynamic alteration was previously obtained for the as-milled $2Mg(NH_2)_2$–3LiH–1/3$LiBH_4$ composite.[32] There, the PCI curve measured at 200 °C also showed a sloped plateau and involved $Li_4(NH_2)_3BH_4$ participation. Considering those results, the difference observed in the ΔH for the LM and LMB sample shows the same tendency.

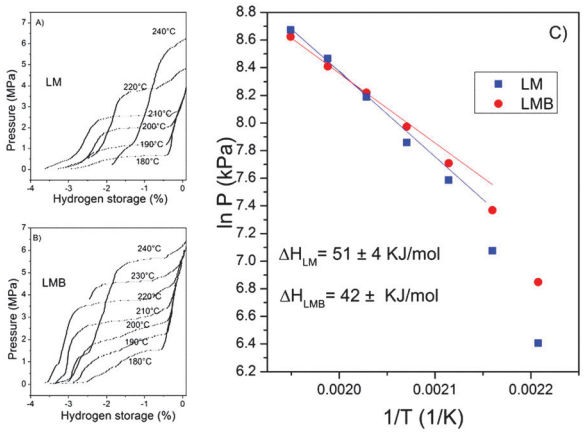

Fig. 7 PCIs of sample LM at different temperatures (A); PCIs of sample LMB at different temperatures (B); calculated dehydrogenation enthalpies of samples LM and LMB (C).

3.5 Role of $Li_4(NH_2)_3BH_4$ in the dehydrogenation of the $Mg(NH_2)_2$–LiH composite

As discussed above, the formation of $Li_4(NH_2)_3BH_4$ was promoted during ball milling (reaction (6)), which is in agreement with previous investigation.[45–47] Furthermore, this compound was also detected by XRPD and FTIR after annealing at 200 °C under 6.0 MPa of hydrogen pressure and after dehydrogenation/rehydrogenation cycles (Table 1). Although its detection at different stages suggests that it only acts as a catalyst (Fig. 4), $Li_4(NH_2)_3BH_4$ participates in different reactions modifying the known two-step dehydrogenation pathway of the $Mg(NH_2)$–2LiH composite (reactions (7) and (8)).[18]

During the first dehydrogenation, $Li_4(NH_2)_3BH_4$ reacted with the excess of MgH_2 present in the initial composite forming $Li_2Mg(NH)_2$ and $LiBH_4$ (reaction (10)). Although this reaction was probably promoted at low equilibrium hydrogen pressure in PCI curves (see Fig. S3, ESI†), it can also occur at the beginning during kinetic dehydrogenation measurements performed at 0.05 MPa of hydrogen (Fig. 2A). Afterwards, the $LiNH_2$ produced by (7) was immediately captured by the $LiBH_4$ produced by (10) in order to form $Li_4(NH_2)_3BH_4$ (reaction (6)), since this reaction has favourable thermodynamics.[28] Then, reactions (6) and (8) could compete among themselves because both require $LiNH_2$ as a starting material. However, the *in situ* formation of $Li_4(NH_2)_3BH_4$ is a fast process due to the fact that $Li_4(NH_2)_3BH_4$ melts and promotes effective mass transfer.

During the second dehydrogenation cycle, as $Li_2Mg_2(NH)_3$ and $Li_4(NH_2)_3BH_4$ are simultaneously present, its interaction is favoured from the beginning (reaction (9)). At the same time, partial dehydrogenation of $Mg(NH_2)_2$ produces $LiNH_2$ (reaction (7)) which reacts with $LiBH_4$ produced by reaction (9). Then, these reactions take place mediated by reaction (6). The removal of $LiNH_2$ and $LiBH_4$ favours both forward reactions (7) and (9), according to Le Chatelier's principle.

Finally, it can be concluded that the formation of $Li_4(NH_2)_3BH_4$ improves the kinetic behaviour in different ways. First, its formation implies the consumption of the intermediate products $LiNH_2$ and $LiBH_4$, promoting reactions (7), (9) and (10) according to Le Chatelier's principle. Second, less energy is required for breaking N–H bonds in $Li_4(NH_2)_3BH_4$ than in $LiNH_2$, which partially justifies the minor activation energy for sample LMB. Third, considering that the rate controlling step for the dehydrogenation of the Li–Mg–N–H system is the diffusion of mobile small ions in both the amide and hydride,[20] the participation of $Li_4(NH_2)_3BH_4$ (a lithium fast-ion conductor) contributes to the Li^+ and H^+ migration.[30]

Moreover, $Li_4(NH_2)_3BH_4$ acts as a reaction medium in the melting state enhancing mass transfer and eliminating the reaction interface. Regarding thermodynamic stability, the exothermic formation of $Li_4(NH_2)_3BH_4$ (reaction (6)) possibly offsets the endothermic effect of dehydrogenation reaction, reducing the desorption enthalpy change.[28] Therefore, these factors operate together to improve the hydrogen storage properties of the $Mg(NH_2)_2$–2LiH composite in the presence of a minor amount of $Li_4(NH_2)_3BH_4$.

4. Conclusions

The effect of $Li_4(NH_2)_3BH_4$ on the hydrogen storage performance of $Mg(NH_2)_2$–2LiH was investigated in the present work. The composite $Mg(NH_2)_2$–2LiH (LM) was synthesized *via* mechanical milling of $2LiNH_2$–MgH_2 and further annealed for 30 min at 200 °C under 6.0 MPa of hydrogen. The phase molar ratio ($Mg(NH_2)_2/LiNH_2$) varied according to the thermal treatment duration, suggesting a reaction displacement with time. Using the same synthesis procedure, the addition of 0.2 $LiBH_4$ facilitated the formation of the $0.7Mg(NH_2)_2$–1.4LiH–$0.2Li_4(NH_2)_3BH_4$ composite (LMB). The new phase $Li_4(NH_2)_3BH_4$ was formed during mechanical milling and no excess of any reactive was detected, inferring that adding $LiBH_4$ could contribute to the formation/recrystallization of $Mg(NH_2)_2$.

Dehydrogenation behaviour after successive cycles shows a beneficial effect of $Li_4(NH_2)_3BH_4$ in the composite under the experimental conditions studied. The dehydrogenation rate in the LMB sample was twice that in the LM sample, whereas hydrogenation can be performed 20 times faster. Although the dehydrogenation rate decreased with the cycle number, the presence of $Li_4(NH_2)_3BH_4$ stabilized the hydrogen storage capacity with cycling. A 9% reduction in the activation energy value due to the presence of $Li_4(NH_2)_3BH_4$ in the Li–Mg–N–H system was observed, which suggests a catalytic effect. Thermodynamic studies of both composites revealed that the first dehydrogenation PCI was different from all the following. For sample LM, the increment in the equilibrium pressure between the first and the second cycle was attributed to the presence of $Li_2Mg_2(NH)_3$, which reveals incomplete rehydrogenation of the system. For sample LMB, the existence of $Li_4(NH_2)_3BH_4$ and its interaction with $Li_2Mg_2(NH)_3$ influenced equilibrium hydrogen pressure and the PCI shape (sloped plateau). The difficulty in achieving thermodynamic conditions leads to a wide range of ΔH values, which does not allow us to ensure thermodynamic destabilization of the system.

Acknowledgements

This study has been partially supported by CONICET (National Council of Scientific and Technological Research), CNEA (National Commission of Atomic Energy), ANPCyT (PICT No. 1052) and Instituto Balseiro (University of Cuyo). The authors thank the Department of Characterization of Materials for the XRD device.

Notes and references

1 G. Walker, *Solid-state Hydrogen storage: Materials and Chemistry*, Woodhead Publishing Limited, England, 2008.
2 R. A. Varin, T. Czujko and Z. Wronski, *Nanomaterials for solid state hydrogen storage*, Springer, New York, 2009.
3 A. Züttel, S. Rentsch, P. Fischer, P. Wenger, P. Sudan, P. Mauron and C. Emmenegger, *J. Alloys Compd.*, 2003, **356**, 515–520.
4 J. J. Vajo, S. L. Skeith and F. Mertens, *J. Phys. Chem. B*, 2006, **74**, 3719–3722.
5 K. Chlopek, C. Frommen, A. Leon, O. Zabara and M. Fichtner, *J. Mater. Chem.*, 2007, **17**, 3496–3503.
6 B. Bogdanovic and M. Schwickardi, *J. Alloys Compd.*, 1997, **253**, 1–9.
7 J. Chen, N. Kuriyama, Q. Xu, H. T. Takeshita and T. Sakai, *J. Phys. Chem. B*, 2001, **105**, 11214–11220.
8 M. Fichtner and O. Fuhr, *J. Alloys Compd.*, 2003, **356**, 418–422.
9 P. Chen, Z. T. Xiong, J. Z. Luo, J. Y. Lin and K. L. Tan, *Nature*, 2002, **420**, 302–304.
10 W. Luo, *J. Alloys Compd.*, 2004, **381**, 284–287.
11 Y. Nakamori, G. Kitahara and S. Orimo, *J. Power Sources*, 2004, **138**, 309–312.
12 Z. Xiong, G. Wu, J. J. Hu and P. Chen, *Adv. Mater.*, 2004, **16**, 1522–1525.
13 W. Luo and E. Rönnebro, *J. Alloys Compd.*, 2005, **404–406**, 392–395.
14 L. Xie, Y. Liu, G. Li and X. Li, *J. Phys. Chem.*, 2009, **113**, 14523–14527.
15 H. Leng, T. Ichikawa and H. Fujii, *J. Phys. Chem. B*, 2006, **110**, 12964–12968.
16 S. Hino, T. Ichikawa, H. Y. Leng and H. Fujii, *J. Alloys Compd.*, 2005, **398**, 62–66.
17 W. Luo, J. Wang, K. Stewart, M. Clift and K. Gross, *J. Alloys Compd.*, 2007, **446**, 336–341.
18 J. Hu, Y. Liu, G. Wu, Z. Xiong and P. Chen, *J. Phys. Chem. C*, 2007, **111**, 18439–18443.
19 Z. T. Xiong, G. T. Wu, J. J. Hu, P. Chen, W. F. Luo and J. Wang, *J. Alloys Compd.*, 2006, **417**, 190–194.
20 Y. Liu, K. Zhong, K. Luo, M. Gao, H. Pan and Q. Wang, *J. Am. Chem. Soc.*, 2009, **131**, 1862–1870.

21 T. Markmaitree and L. L. Shaw, *J. Power Sources*, 2010, **195**, 1984–1991.
22 C. Li, Y. F. Liu, Y. J. Gu, M. X. Gao and H. G. Pan, *Chem. – Asian J.*, 2013, **8**, 2136–2143.
23 C. Liang, Y. F. Liu, M. X. Gao and H. G. Pan, *J. Mater. Chem. A*, 2013, **1**, 5031–5036.
24 Y. F. Liu, C. Li, B. Li, M. X. Gao and H. G. Pan, *J. Phys. Chem. C*, 2013, **117**, 866–875.
25 J. H. Wang, T. Liu, G. T. Wu, W. Li, Y. F. Liu, C. M. Araujo, R. H. Scheicher, A. Blomqvist, R. Ahuja and Z. T. Xiong, *Angew. Chem., Int. Ed.*, 2009, **48**, 5828–5832.
26 J. J. Hu, M. Fichtner and P. Chen, *Chem. Mater.*, 2008, **20**, 7089–7094.
27 J. J. Hu, Y. F. Liu, G. T. Wu, Z. T. Xiong, Y. S. Chua and P. Chen, *Chem. Mater.*, 2008, **20**, 4398–4402.
28 J. Yang, A. Sudik, D. J. Siegel, D. Halliday, A. Drews, R. O. Carter, C. Wolverton, G. J. Lewis, J. W. Sachtler and J. W. Low, *Angew. Chem., Int. Ed.*, 2008, **47**, 882–887.
29 Y. Zhang, Z. Xiong, H. Cao, G. Wu and P. Chen, *Int. J. Hydrogen Energy*, 2014, **39**, 1710–1718.
30 H. G. Pan, S. B. Shi, Y. F. Liu, B. Li, Y. J. Yang and M. X. Gao, *Dalton Trans.*, 2013, **42**, 3802–3811.
31 B. Li, Y. F. Liu, J. Gu, Y. J. Gu, M. X. Gao and H. G. Pan, *Int. J. Hydrogen Energy*, 2013, **38**, 5030–5038.
32 H. J. Cao, G. T. Wu, Y. Zhang, Z. T. Xiong, J. S. Qiu and P. Chen, *J. Mater. Chem. A*, 2014, **2**, 15816–15822.
33 P. A. Anderson, P. A. Chater, D. R. Hewett and P. R. Slater, *Faraday Discuss.*, 2011, **151**, 271–284.
34 B. Li, Y. Liu, C. Li, M. Gao and H. Pan, *J. Mater. Chem. A*, 2014, **2**, 3155–3162.
35 N. S. Gamba, P. Arneodo Larochette and F. C. Gennari, *RSC Adv.*, 2015, **5**, 68542–68550.
36 N. S. Gamba, P. Arneodo Larochette and F. C. Gennari, *RSC Adv.*, 2016, **19**, 15622–15629.
37 L. Fernández Albanesi, P. Arneodo Larochette and F. C. Gennari, *Int. J. Hydrogen Energy*, 2013, **38**, 12325–12334.
38 L. Fernández Albanesi, S. Garroni, P. Arneodo Larochette, P. Nolis, G. Mulas, S. Enzo, M. D. Baró and F. C. Gennari, *Int. J. Hydrogen Energy*, 2015, **40**, 13506–13517.
39 L. Fernández Albanesi, S. Garroni, S. Enzo and F. C. Gennari, *Dalton Trans.*, 2016, **45**, 5808–5814.
40 H. M. Rietveld, *J. Appl. Crystallogr.*, 1969, **2**, 65–71.
41 J. Rodríguez-Carvajal, *Phys. B*, 1993, **192**, 55–69.
42 C. Liang, M. X. Gao, H. G. Pan and Y. F. Liu, *Appl. Phys. Lett.*, 2014, **105**, 083909.
43 J. Hu, W. Eveline, M. Hoelzel and M. Fichtner, *Dalton Trans.*, 2010, **39**, 9100–9107.
44 Z. Xiong, J. Hu, G. Wu, P. Chen, W. Luo, K. Gross and J. Wang, *J. Alloys Compd.*, 2005, **398**, 235–239.
45 P. A. Chater, W. I. F. David, S. R. Johnson and P. P. Edwards, *Chem. Commun.*, 2006, 2439–2441.
46 F. E. Pinkerton and M. S. Meyer, *J. Phys. Chem. C*, 2009, **113**, 11172–11176.
47 G. P. Meisner, M. L. Scullin, M. Balogh, F. E. Pinkerton and M. S. Meyer, *J. Phys. Chem. B*, 2006, **110**, 4186–4192.